J|A|C|S
ARTICLES
Published on Web 02/28/2004

Self-Assembly of Electron Donor−Acceptor Dyads into Ordered Architectures in Two and Three Dimensions: Surface Patterning and Columnar "Double Cables"

Paolo Samorì,*[,†,‡,§] Xiaomin Yin,[†] Natalia Tchebotareva,[||,⊥] Zhaohui Wang,[||] Tadeusz Pakula,[||] Frank Jäckel,[†] Mark D. Watson,*[,◇,||] Alessandro Venturini,[‡] Klaus Müllen,*[,||] and Jürgen P. Rabe*[,†]

Contribution from the Department of Physics, Humboldt University Berlin, Newtonstrasse 15, D-12489 Berlin, Germany, Institute for Organic Synthesis and Photoreactivity, Consiglio Nazionale della Ricerche, via Gobetti 101, 40129 Bologna, Italy, Laboratory of Nanochemistry, Institut de Science et d'Ingènierie Supramolèculaires (ISIS), Université Louis Pasteur, 8 allée Gaspard Monge, BP 70028, F-67083, Strasbourg, France, and Max Planck Institute for Polymer Research, Postfach 3148, D-55021 Mainz, Germany

Received September 22, 2003; E-mail: samori@isof.cnr.it; mdwatson@uky.edu; muellen@mpip-mainz.mpg.de; rabe@physik.hu-berlin.de

Abstract: We report the synthesis and characterization of covalent dyads and multiads of electron acceptors (A) and donors (D), with the purpose of exploiting their nanophase separation behavior toward (a) two-dimensional (2D) surface patterning with well-defined integrated arrays of dissimilar molecular electronic features and (b) bulk self-assembly to noncovalent columnar versions of the so-called "double cable" systems, the likes of which could eventually provide side-by-side percolation pathways for electrons and holes in solar cells. Soluble, alkylated hexa-*peri*-hexabenzocoronenes (HBCs) bearing tethered anthraquinones (AQs) are shown by scanning tunneling microscopy (STM) to self-assemble at the solution−graphite interface into either defect-rich polycrystalline monolayers or extended 2D crystalline domains, depending on the number of tethered AQs. In the bulk, the thermal stability of the room-temperature HBC columnar phase is increased, which is attributed to the desired nanotriphase separation of HBC columns, insulating alkyl sheaths, and AQ units. Homeotropic alignment (columns normal to surfaces), predicted to be ideal for potential exploitation of such "double cables" in photovoltaic devices, is demonstrated.

Introduction

The pioneering vision of Aviram and Ratner of a molecular rectifier, based on an intrinsically electronically asymmetric π-donor-σ-unit-π-acceptor dyad,[1] has prompted great activity focused on the synthesis and characterization of more and more complex donor−acceptor molecules aimed at the generation of new electronic devices.[2] However, rectification has been experimentally observed also with symmetric molecules located between a scanning tunneling microscopy (STM) tip and a conducting substrate, which has been attributed to positional and energetic asymmetries of the molecule within the junction and its molecular orbitals with respect to the Fermi levels of the electrodes.[3] Donor−acceptor (D−A) dyads could be exploited in this geometry to construct well-defined integrated two-dimensional (2D) arrays of dissimilar rectifying elements.[4] In addition to obvious implications for future development of multicomponent nanoscale devices relying solely on self-assembly for their construction, such arrays would allow the simultaneous study of the electronic properties of differing π-systems at the (sub)molecular level, minimizing variables inherent to separate experiments on the individual components.

High-performance bulk organic electronic devices can be developed by using, as active components, π-conjugated molecules.[5] Besides the already established light-emitting diodes,[6] a great deal of attention has recently been paid to solar

* Corresponding author fax numbers: P.S., (+39) 051-6399844; M.D.W., (+1) 859-257-8459; K.M., (+49) 6131-379350; J.P.R., (+49) 30-20937632.
† Humboldt University Berlin.
‡ CNR Bologna.
§ Université Louis Pasteur.
|| Max Planck Institute for Polymer Research.
⊥ Present address: Department of Chemical Engineering and Chemistry, Eindhoven University of Technology, 5600 MB Eindhoven, The Netherlands.
◇ Present address: Department of Chemistry, University of Kentucky, Lexington, Kentucky 40506-0055.

(1) Aviram, A.; Ratner, M. *Chem. Phys. Lett.* **1974**, *29*, 277−283.
(2) (a) Metzger, R. M. *Acc. Chem. Res.* **1999**, *32*, 950−957. (b) Davis, W. B.; Svec, W. A.; Ratner, M. A.; Wasielewski, M. R. *Nature* **1998**, *396*, 60−63. (c) Joachim, C.; Gimzewski, J. K.; Aviram, A. *Nature* **2000**, *408*, 541−548.
(3) (a) Stabel, A.; Herwig, P.; Müllen, K.; Rabe, J. P. *Angew. Chem., Int. Ed. Engl.* **1995**, *34*, 1609. (b) Troisi, A.; Ratner M. A. *J. Am. Chem. Soc.* **2002**, *124*, 14528−14529.
(4) Jäckel, F.; Wang, Z.; Watson, M. D.; Müllen, K.; Rabe. J. P. *Chem. Phys. Lett.* (submitted for publication).
(5) (a) Petty, M. C.; Bryce, M. R.; Bloor, D.; Eds. *Introduction to Molecular Electronics*; Oxford University Press: New York, 1995. (b) Aviram, A.; Ratner, R.; Eds. Molecular Electronics: Science and Technology; *Ann. N.Y. Acad. Sci.* **1998**, *852*. (c) Alivisatos, A. P.; Barbara, P. F.; Castleman, A. W.; Chang, J.; Dixon, D. A.; Klein, M. L.; McLendon, G. L.; Miller, J. S.; Ratner, M. A.; Rossky, P. J.; Stupp, S. I.; Thompson, M. E. *Adv. Mater.* **1998**, *10*, 1297. (d) Cahen, D.; Hodes, G. *Adv. Mater.* **2002**, *14*, 789−798. (e) Aviram, A., Ratner, R., Mujica, V., Eds. Molecular Electronics II; *Ann. N.Y. Acad. Sci.* **2002**, *960*.

Chart 1

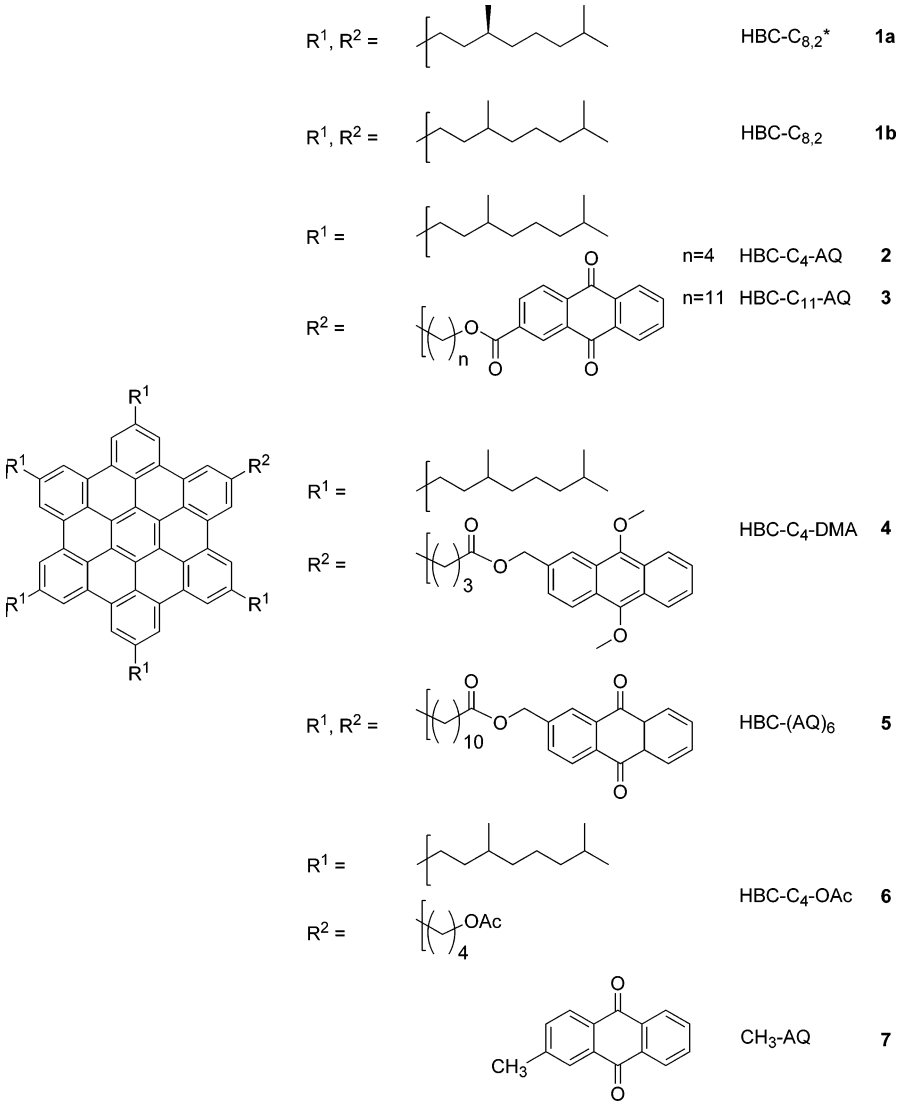

cells.[7] A proposed optimal morphology is the interpenetrating network of electron acceptors and donors providing complementary percolation pathways connecting two electrodes.[7b,c] Achieving full control over the structural order and driving the self-organization toward nanosegregated structures is a viable approach to increase the external quantum efficiency. Here, covalent D−A dyads represent an alternative to blends; the so-called "double cable" approach[7b] maximizes the bulk p−n junction by limiting phase separation to the nanoscale. While these "double cable" systems are based on conjugated polymers as hole-transport media, we have started to focus on columnar discotic mesogenic units, as their tendency to long-range homeotropic alignment, if persistent in double-cable hybridized systems, should lead to highly one-dimensional transport.

As an electron-rich mesogenic unit for both columnar phase formation and patterning of surfaces, hexa-*peri*-hexabenzocoronene (HBC) can be designed and synthesized with different substituents (Chart 1),[8] permitting control of the electronic and self-assembly properties of the single molecule. In addition to the above-mentioned molecular rectification in the junction between STM tip and HOPG,[3a] the supramolecular columnar architectures based on $\pi-\pi$ stacked HBCs have been found to possess the highest charge carrier mobility among discotic systems.[9] Recently we described an HBC−pyrene dyad that provided both large area nanophase separated patterning at the solution−solid interface and nanophase separation in the bulk columnar phase.[10] Here we replaced pyrene with the strong electron acceptor anthraquinone (AQ). Due to their combined optoelectronic properties, these systems are not expected to efficiently harvest the solar spectrum, but instead they serve as models and the next step toward the goal of organic photovoltaic devices based on columnar "double cables". We describe the

(6) Friend, R. H.; Gymer, R. W.; Holmes, A. B.; Burroughes, J. H.; Marks, R. N.; Taliani, C.; Bradley, D. D. C.; Dos Santos, D. A.; Brèdas, J. L.; Lögdlund, M.; Salaneck, W. R. *Nature* **1999**, *397*, 121.

(7) (a) Eckert, J.-F.; Nicoud, J.-F.; Nierengarten, J.-F.; Liu, S.-G.; Echegoyen, L.; Armaroli, N.; Barigelletti, F.; Ouali, L.; Krasnikov, V.; Hadziioannou, G. *J. Am. Chem. Soc.* **2000**, *122*, 7467−7479. (b) Cravino, A.; Sariciftci, N. S. *J. Mater. Chem.* **2002**, *12*, 1931−1943. (c) Schmidt-Mende, L.; Fechtenkötter, A.; Müllen, K.; Moons, E.; Friend, R. H.; MacKenzie, J. D. *Science* **2001**, *293*, 1119−1123. (d) El-ghayoury, A.; Schenning, A. P. H. J.; van Hal, P. A.; van Duren, J. K. J.; Janssen, R. A. J.; Meijer, E. W. *Angew. Chem., Int. Ed.* **2001**, *40*, 3660−3663. (e) Pourtois, G.; Beljonne, D.; Cornil, J.; Ratner, M. A.; Brédas, J. L. *J. Am. Chem. Soc.* **2002**, *124*, 4436−4447.

(8) Ito, S.; Wehmeier, M.; Brand, J. D.; Kubel, C.; Epsch, R.; Rabe, J. P.; Mullen, K. *Chem. Eur. J.* **2000**, *6*, 4327−4342.

(9) van de Craats, A. M.; Warman, J. M. *Adv. Mater.* **2001**, *13*, 130−133. Schultz, A.; Laschat, S.;. Abbott, A. P.; Langner, M.; Reeve, T. B. *J. Chem. Soc., Perkin Trans.* **2000**, *1*, 3356−3361.

(10) Tchebotareva, N.; Yin, X.; Watson, M. D.; Samorì, P.; Rabe, J. P.; Müllen, K. *J. Am. Chem. Soc.* **2003**, *125*, 9734−39.

Scheme 1. Syntheses of HBC−AQ Dyads **2** and **3** and Reference HBC Ester **6**[a]

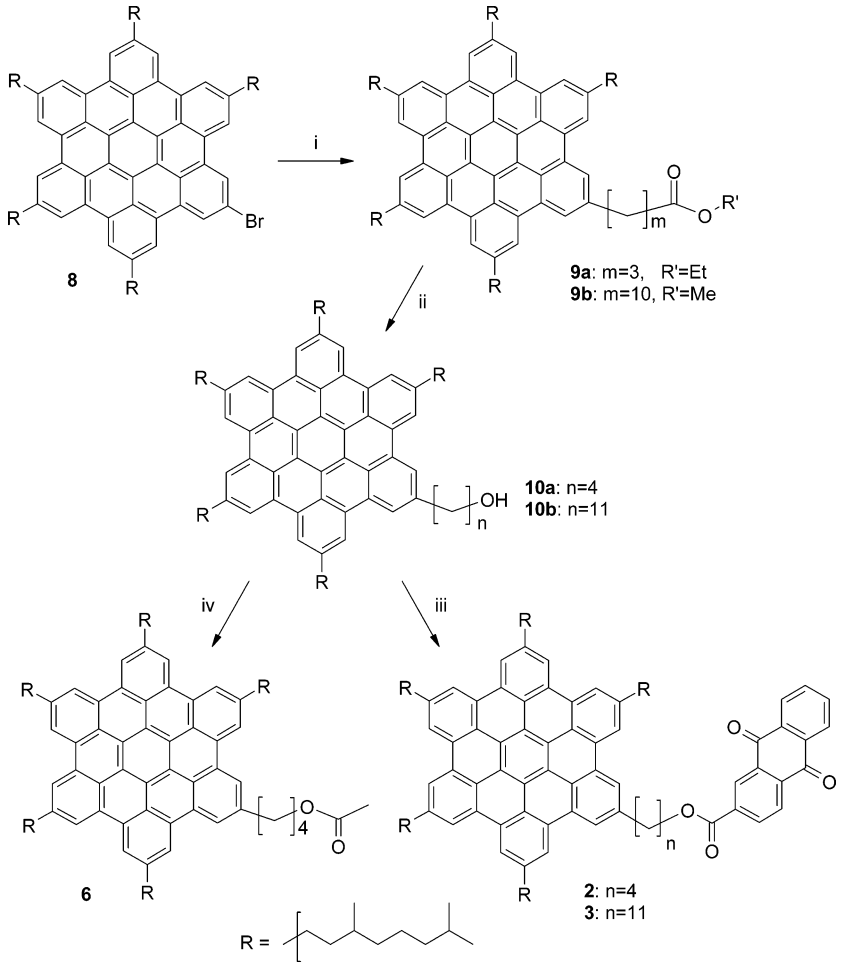

[a] (i) $IZn(CH_2)_mCO_2R'$, $Cl_2Pd[dppf]\cdot MeCl_2$, THF; (ii) $LiAlH_4$, THF; (iii) AQ-2-CO_2H, EDC, DMAP, $MeCl_2$; (iv) AcCl, pyridine, THF.

synthesis and the physicochemical characterization of HBC−AQ-based donor−acceptor dyads, connected by alkyl tethers of two different lengths, as well as of an HBC bearing six tethered AQ units. While the properties in three dimensions have been studied by differential scanning calorimetry (DSC), wide-angle X-ray diffraction (WAXD), and polarized optical microscopy (POM), the 2D self-assembly at a solid−liquid interface was investigated with scanning tunneling microscopy (STM). In both 2D and 3D, the effect of the AQ units is compared for two HBC derivatives, one bearing only solubilizing alkyl chains, and a second bearing a tethered dimethoxyanthracene (DMA) unit.

Results and Discussion

Synthesis. The synthesis of the HBC−anthraquinone dyads (**2** and **3**) was carried out as illustrated in Scheme 1. Similar to the published synthesis of alcohol **10a**,[10] Negishi-type of coupling of bromo-HBC **8**[11] with 10-(methoxycarbonyl)decyl-1-zinc iodide[12] followed by reduction with $LiAlH_4$ provided **10b**. Finally, carbodiimide-promoted esterification of **10a,b** with 9,-10-anthraquinone-2-carboxylic acid yielded the desired targets **2** and **3**. Acetylation of **10a** provided model HBC **6**, with a similar substitution pattern but without AQ units. To ascertain the effect of the bulkiness and electronic nature of the tethered unit, HBC−DMA dyad **4** was prepared by coupling of 2-hydroxymethyl-9,10-dimethoxyanthracene[13] with HBC acid **11**, obtained via alkali hydrolysis of **9a** (Scheme 2). Synthesis of hexaanthraquinone-functionalized HBC derivative **5** was carried out by esterification of hexaacid HBC (**12**)[14] with commercially available 2-hydroxymethyl-9,10-dimethoxyanthraquinone (see Scheme 3).

Self-Assembly at Surfaces. Figure 1, panels a and b, show STM current images of self-assembled architectures of HBC−AQ dyads **2** and **3**, respectively. They reveal polycrystalline structures consisting of bright spots arranged according to a hexagonal motif. These bright spots (corresponding to high tunneling current) can be assigned to the HBC π-conjugated cores, since the energy difference between their highest occupied molecular orbitals (HOMOs) and the Fermi level of the graphite substrate is rather small (Figure 2)[15] The aliphatic side chains, which are positioned in the darker parts of the image, could not be resolved, probably because of their high conformational mobility on a time scale faster than the STM imaging. The

(11) Fechtenkötter, A.; Tchebotareva, N.; Watson, M. D.; Müllen, K. *Tetrahedron* **2001**, *57*, 3769−3783.
(12) Hu, Y.; Yu, J.; Yang, S.; Wang, J.-X.; Yin, Y. *Synth. Commun.* **1998**, *28*, 2793−2800.
(13) Jiang, H.; Xu, H. J.; Ye, J. P. *J. Chem. Soc., Perkin Trans. 2* **2000**, *5*, 925−930.
(14) Brand, J. D.; Kübel, C.; Ito, S.; Müllen, K. *Chem. Mater.* **2000**, *12*, 1638−1647.
(15) Lazzaroni, R.; Calderone, A.; Brédas, J. L.; Rabe, J. P. *J. Chem. Phys.* **1997**, *107*, 99−105.

Scheme 2. Synthesis of HBC−DMA Dyad **4**[a]

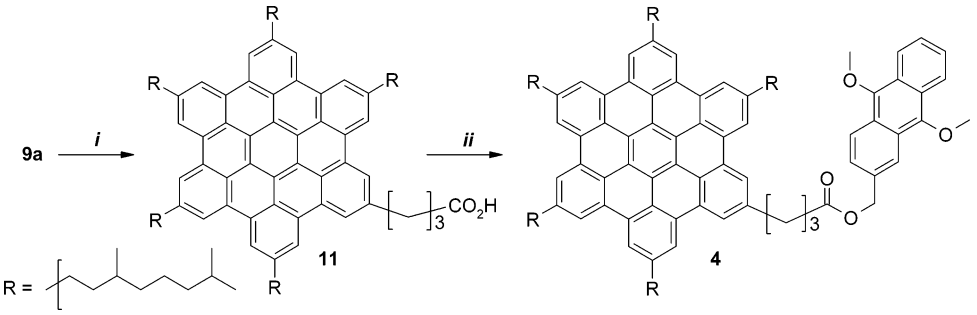

[a] (i) KOH, H_2O, THF; (ii) 9,10-dimethoxyanthracene-2-CH_2OH, EDC, DMAP, $MeCl_2$.

Scheme 3. Synthesis of Hexa-AQ-Substituted HBC **5**[a]

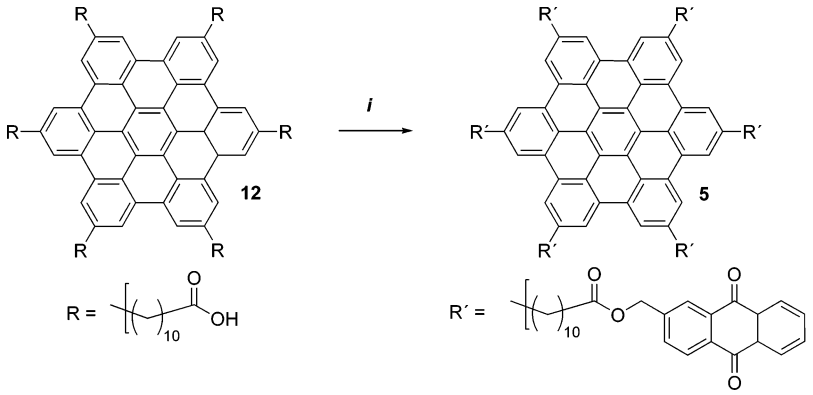

[a] (i) 2-($HOCH_2$)-AQ, EDC, DMAP, $MeCl_2$.

domains exhibit two energetically equivalent orientations, at roughly +15° and −15°, with respect to the underlying substrate lattice. Thus each of the two can be regarded as a mirror image with respect to a graphite axis.

From the size of the unit cell, one can roughly estimate that for both **2** and **3** the HBC core plus three methylene units per side chain are packed on the substrate as already reported for **1a**.[16,10] In fact, the methyl branch at the γ carbon is likely to sterically hinder the packing of the chain's tail on the surface, inducing its solubilization in the supernatant solution. At a first glance, the high similarity in the arrangement of **1**−**3** in terms of unit cell size (Table 1), image contrast, and packing symmetry suggests that the side chains bearing the AQ units do not play a prime role in the self-assembly process. However, **2** and **3** display neither the perfect 2D hexagonal crystals of **1a**, which were extended over more than a 50 × 50 nm^2 area,[16] nor the defect-poor nanophase segregated arrangement observed for an HBC−pyrene dyad (parallel HBC and pyrene double rows).[10] Instead large defect areas (Figure 1c,d), as detailed below, are observed here. The several defects viewed in **2** and **3** architectures on graphite are not due to defects in the substrate underneath, which is nearly defect-free. This is proven by the absence of such defects on many other (supra)molecular species self-assembled on HOPG.[17] This indicates that some other factors, e.g., the solvation and the electronic properties of the AQ side group, influence the self-assembly at the solution−HOPG interface. For **2** the domains exhibit anisotropic shapes (indicated by black arrows in Figure 1a), consisting of a dimerlike structure, which appear to be a segment of the hexagonal 2D crystal. The domain boundaries convey single-row-like void defects (marked with white arrows in Figure 1a) every third row. On the other hand, the zoom-out for molecule **3** shown in Figure 1d displays again a polycrystalline structure but characterized by double-row-like void defects. Additionally, the domain size can be extended to four rows and sometimes even six. It is noteworthy that short gap defects (less than six missing molecules) are often observed rather than the longer ones (more than nine), which is again different from **2**.

It is well-known that long alkanes or alkyl chains tend to physisorb on graphite from solutions in an all-trans conformation,[18] maximizing the enthalpic gain upon adsorption, amounting to ∼2 kcal/mol per methylene unit.[19] Differently from the reference compound **1** containing six branched alkyl side groups, both **2** and **3** have one linear bridge between HBC core and AQ side group, which breaks the molecular symmetry. It is reasonable to expect more and/or larger defects in the case of **3** than of **2** due to the longer alkyl bridge.[20] Instead, **3** provides more extended hexagonal packing with seldom dimerlike crystalline row motif compared to **2**. Counting the bright spots in the STM images, we quantified the degree of surface coverage (Table 1). At the interface coated with **2**, only 28 isolated dimer pairs can be observed within an image, whereas only 38 molecules (less than 7%) have six neighbors. Differently, for

(16) Samorí, P.; Fechtenkötter, A.; Böhme, T.; Jäckel, F.; Müllen, K.; Rabe, J. P. *J. Am. Chem. Soc.* **2001**, *123*, 11462−11467.
(17) For reviews see (a) Cyr, D. M.; Venkataraman, B.; Flynn, G. W. *Chem. Mater.* **1996**, *8*, 1600−1615. (b) Samorì, P.; Rabe, J. P. *J. Phys.: Condens. Matter.* **2002**, *14*, 9955−9973. (c) De Feyter, S.; De Schryver, F. C. *Chem. Soc. Rev.* **2003**, *32*, 139−150.
(18) (a) McGonigal, G. C.; Bernhadt, R. H.; Thomson, D. *J. Appl. Phys. Lett.* **1990**, *57*, 28. (b) Rabe, J. P.; Buchholz, S. *Science* **1991**, *253*, 424. (c) Cyr, D. M.; Venkataraman, B.; Flynn, G. W. *Chem. Mater.* **1996**, *8*, 1600.
(19) Hentschke, R.; Schürmann, B. L.; Rabe, J. P. *J. Chem. Phys.* **1992**, *96*, 6213−6221.
(20) Qiu, X. H.; Wang, C.; Zeng, Q. D.; Xu, B.; Yin, S. X.; Wang, H. N.; Xu, S. D.; Bai, C. L. *J. Am. Chem. Soc.* **2000**, *122*, 5550.

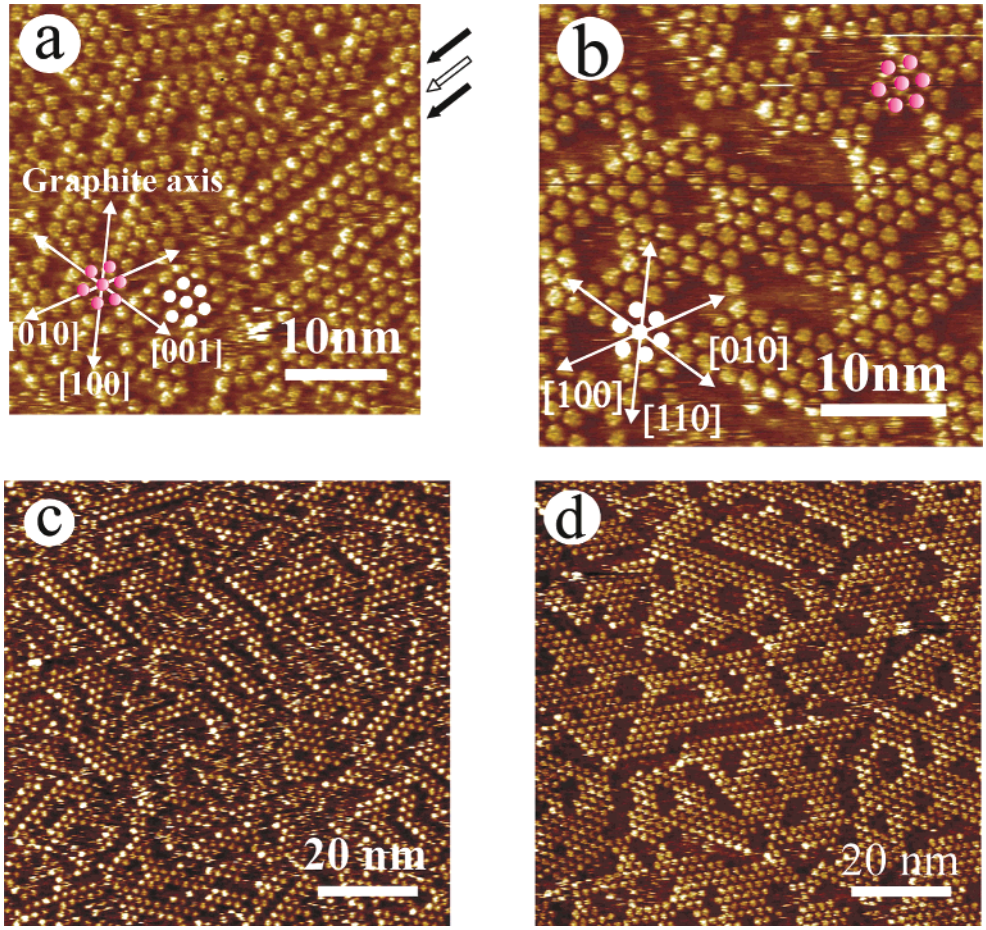

Figure 1. STM current images of HBC−AQs on HOPG. Tip bias voltage $U_t = -1.2$ V; average tunneling current $I_t = 0.1$ nA. (a) HBC−C_4−AQ **2**; black arrows indicate dimer pattern while the white arrow marks a single-row defect. (b) HBC−C_{11}−AQ **3**; white and magenta hexagonal spot assemblies stand for two different orientations. Survey images of the polycrystalline arrangements are shown for molecules (c) **2** and (d) **3**.

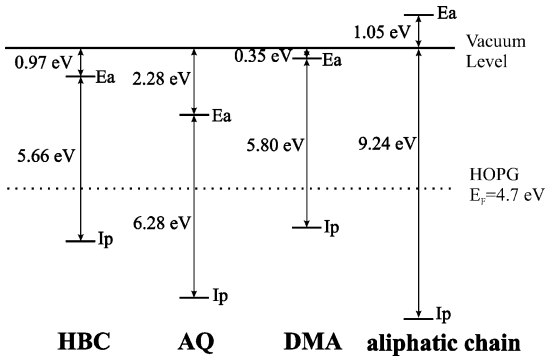

Figure 2. Scheme of the adiabatic electron affinities (E_a) and ionization potentials (I_p) for HBC, AQ, DMA, and aliphatic chain ($C_{10}H_{22}$) in vacuo, as calculated with full density functional optimizations. Since the experimental results have been obtained in the condensed phase, for the interpretation of the STM contrasts they have to be considered only for the trend in the energy differences of the levels.

3, 153 out of 500 molecules (~30%) are assembled with six HBC nearest neighbors.

HBC−DMA dyad **4** packs at the solid−liquid interface in a hexagonal arrangement (Figure 3) similar to the model system **1a** bearing no tethered π-system. Again two energetically equivalent cells oriented at ±15° relative to HOPG have been found. The domain size extends to several hundreds of nanometers, with only few point defects. Thus the bulky DMA unit has little effect on the packing behavior of the HBC cores, most probably because it prefers to extend into the supernatant solution rather than packing on HOPG. The STM image of **4** indicates that the apparent void defects in the hexagonal packing of the HBC cores of **2** and **3** are not simply dislocations due to lowered molecular symmetry and tethering of a bulky unit. In fact, the methylation of the oxygen atoms of AQ to give DMA not only increases the bulkiness of the tethered π-system but also changes it from electron-poor to electron-rich (see Figure 2), two factors that surely affect their affinity and packing efficiency on the graphite surface.

Figure 4 shows the STM current images of the hexaanthraquinone-substituted HBC **5** [HBC−$(AQ)_6$]. It reveals highly regular patterning with only a few point defects. Here the unit cell is rectangular with the short vector of the unit cell, *a*, aligned along one HOPG crystallographic axis, reducing the packing symmetry from 3-fold, which is observed locally for the HBC cores of **1**−**3** and an HBC−pyrene dyad,[10] to 2-fold, as reported for HBCs carrying only unbranched alkyl chains.[3a] The symmetry operations related to the hexagonal HOPG lattice lead to three energetically equivalent orientations of the unit cell. The determined unit cell area of $A = 8.8 \pm 0.4$ nm^2 does not fulfill the spatial requirement of a single molecule lying completely flat on the graphite surface (9.50 nm^2). However, it is larger than the expected van der Waals contour if we assume all AQs to be oriented perpendicular to the basal plane of graphite, which would lead to an area of 7.2 nm^2. Investigating the molecular arrangement more carefully, additionally to the spots ascribed

Table 1. Unit Cell Parameters and Details on the Arrangements in 2D

	a (nm)	*b* (nm)	α (deg)	area (nm^2)	hexa cov (%)
HBC−$C_{8,2}$,[16] **1a**	1.86 ± 0.10	2.03 ± 0.10	58 ± 2	3.20 ± 0.36	∼100
HBC−C_4−AQ, **2**	1.86 ± 0.10	1.85 ± 0.09	58 ± 3	2.9 ± 0.4	7
HBC−C_{11}−AQ, **3**	1.84 ± 0.12	1.80 ± 0.09	61 ± 3	2.9 ± 0.4	30
HBC−C_4−DMA, **4**	1.84 ± 0,10	1.84 ± 0.10	60 ± 1	2.9 ± 0.4	
HBC−$(AQ)_6$, **5**	2.44 ± 0.05	3.59 ± 0.08	90 ± 2	8.8 ± 0.4	

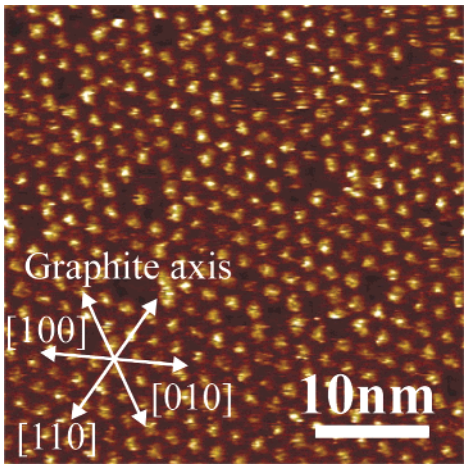

Figure 3. STM current image of HBC−C_{11}−DMA **4**. $U_t = -1.2$ V; $I_t = 0.1$ nA.

to the HBC cores, smaller bright areas have been found within the rectangular unit cell. The three zoom-in images of Figure 4a, shown in Figure 4b−d, provide better evidence of these smaller bright spots. In line with the quantum chemical calculations (Figure 2), these features, that are located on the diagonals of the unit-cell between two HBC cores and that are characterized by a smaller tunneling current than the HBC cores, can be attributed to AQ moieties packed on the HOPG surface. Considering the aforementioned space requirements of the molecule under study, the observation suggests that four AQs are immobilized on the graphite surface. Furthermore, the simultaneous observation of these bright areas in multiple domains with differing orientations within the same image makes it unlikely that they stem from an artifact and ensures that the AQs are indeed located only on the diagonals of the unit cell. The present exploration did not provide direct evidence on the behavior of the remaining AQs, but they most likely extend into the supernatant solution.

Considering the case of **2** and **3**, although the STM current images did not provide unambiguous evidence of the packing of the AQ side groups, three possibilities shall be discussed here:

(a) All AQ units are solubilized in the supernatant organic solution;

(b) AQ packs inter- or intramolecularly on top of neighboring HBCs to form D−A double layers; or

(c) AQ packs directly on the HOPG substrate.

Scenario (a) can be rejected outright on the basis of comparison to the near-perfect hexagonal packing of HBC−DMA **4**, which most likely does follow from scenario a (fully solvated tethered units giving a molecular footprint with the highest possible symmetry).[16] According to the almost identical chemical structures of **2** and **3**, one could also hardly explain their differences in hexagonal surface coverage. This is further supported by the highly regular packing of the tethered AQ functionalities of HBC−$(AQ)_6$ **5** on the surface. We can therefore conclude that solvation plays some, but not the only, role for **2** and **3**.

Either packing model in scenario (b) is characterized by the formation of D−A bilayers, accompanied by an enthalpic gain[21] different from that obtained by AQ adsorption on HOPG. HBC and AQ do in fact exhibit D−A interactions in solution, as indicated by absorption/fluorescence measurements (Supporting Information). It is important to point out again that the hexagonal surface coverage is smaller for **2** than for **3**. In the former case, the center-to-center distance between the HBC core and the AQ amounts to 1.8 nm for an all-trans conformation of the alkyl bridge, which is very close to the experimentally observed hexagonal unit cell vector (1.84 nm). On the contrary, a longer spacer, such as the one of **3**, allows both inter- and intramolecular D−A complexes at the surface. STS investigations (not shown here) did not indicate in any way the presence of D−A stacks, in opposition to this scenario. However, since strong tip−sample interactions might disrupt D−A stacks, their existence cannot be rigorously excluded.

Scenario (c), on the other hand, takes into account the tendency of the AQs to pack on the surface, which is evidenced by the STM results of the hexasubstituted HBC **5**. For the monosubstituted **2** and **3**, the size of the defects in hexagonal packing is directly related to the length of the alkyl tethers carrying the AQ, while the number of defects results from the competition between the packing of AQ and the close hexagonal packing of the HBC on the HOPG surface. This competition results in a subtle balance in the enthalpic gains associated with the adsorption of AQ and HBC on HOPG, leading to a more loosely packed arrangement compared to monolayers of **1a**. In addition to the aforementioned competition, one should consider that we could not form stable monolayers from a model alkyl ester AQ derivative using 1,2,4-trichlorobenzene but could with 1-phenyloctane as solvent. Furthermore, not only did a previous STM study[22] of a related alkylated AQ reveal dimorphism (two different packing arrangements) but also one of these arrangements was proposed to be the dynamic average of a further two resulting from oscillation of the AQ units between edge-on and face-on packing and concomitant lateral sliding of the molecules. This enhanced dynamics resulting from an equilibrium between solvated and adsorbed AQs clearly hinders long-range order, particularly in the competitive solvent, and might also explain why the AQ units could not be visualized in the void defects. Together with a distinct size mismatch between cross-sections of the tethered components (poor space filling), a weak affinity for HOPG proves overly disruptive. The essentially identical size mismatch in the previously published HBC−pyrene dyad did not prevent self-assembly to ordered 2D crystals, most likely

(21) Hunter, C. A.; Lawson, K. R.; Perkins, J.; Urch, C. J. *J. Chem. Soc., Perkin Trans. 2* **2001**, 651−669.
(22) Stabel, A.; Heinz, R.; Rabe, J. P.; Wegner, G.; De Schryver, F. C.; Corens, D.; Dehaen, W.; Süling, C. *J. Phys. Chem.* **1995**, *99*, 8690−97.

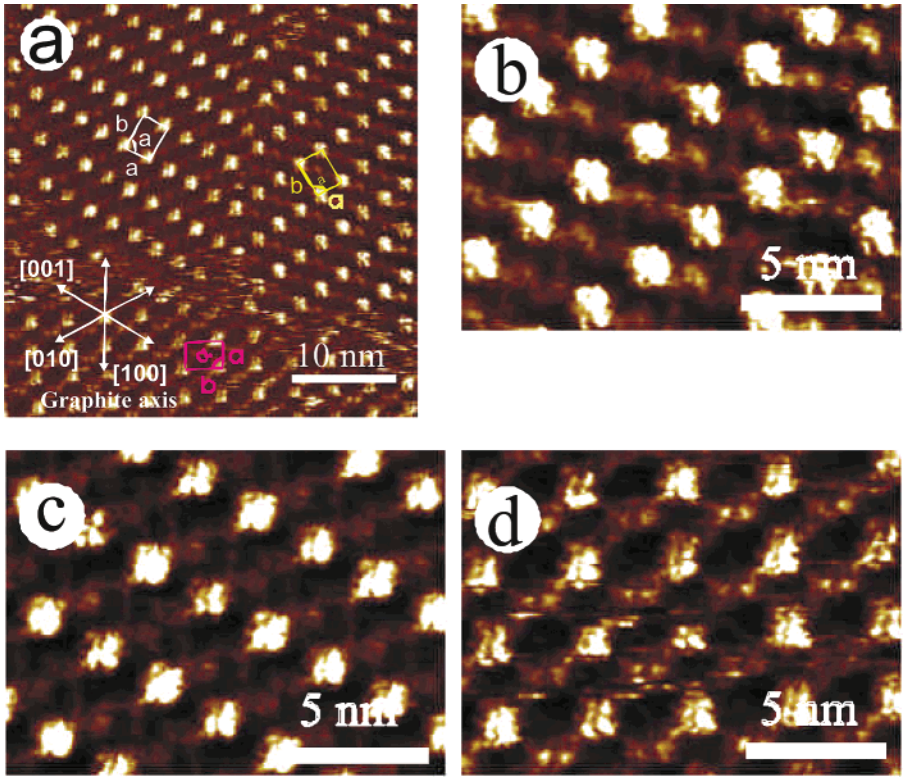

Figure 4. STM current images of HBC−(AQ)$_6$ **5**. $U_t = -1.2$ V; $I_t = 0.1$ nA. (a) Large scale with three different orientations indicated with white, magenta, and green individually. (b) Zoom-in image of the upper left domain. (c) Zoom-in image of the upper right domain. (d) Zoom-in image of the lower left domain.

due to a greater affinity of pyrene for HOPG. The larger ratio of AQ units per HBC core in **5** (six AQs compared to one in the dyads) allows for more equitable space filling, which must compensate for the decreased tendency for adsorption, leading to extended single-crystalline 2D domains. Possible contribution to this stabilization by adsorption of the nonbranched alkyl tethers of **5** should not be ignored.

Bulk Properties. All compounds were extruded into fibers, from which 2D WAXD transmission measurements clearly indicate columnar structures with coinciding columnar and fiber axes. All WAXD patterns have the following features typical of columnar (meso)phases: (a) a diffuse halo at $d \sim 0.42$ nm arising from the liquidlike portions of the alkyl chains, (b) equatorial reflections arising from the 2D lattice describing the intercolumnar packing, and (c) arcs on the meridian with d spacing corresponding to the intracolumnar (stacking) repeating distance.

The DSC thermograms of **1b**, **2**, **3**, and **5** are compared in Figure 5 and the thermal transitions, together with their assignments from WAXD and POM, are collected in Table 2. For all HBC−AQ couples, the isotropization temperature (T_i) is substantially lowered compared to model compound **1b**. Simple desymmetrization is not the cause, as in the case of **6**, which actually shows a slightly increased T_i relative to **1b**, due to one less bulky branched chain. The more bulky DMA unit in **4** depresses the T_i less than the AQ in the structurally similar HBC−C_4−AQ **2**. We propose then that the T_i is lowered in the HBC−AQ compounds not simply because of the entropic disruption of the mesophase by a bulky tethered unit or due to increased thermal fluctuations in the intercolumnar distance associated with reduced symmetry but because the flat AQ units

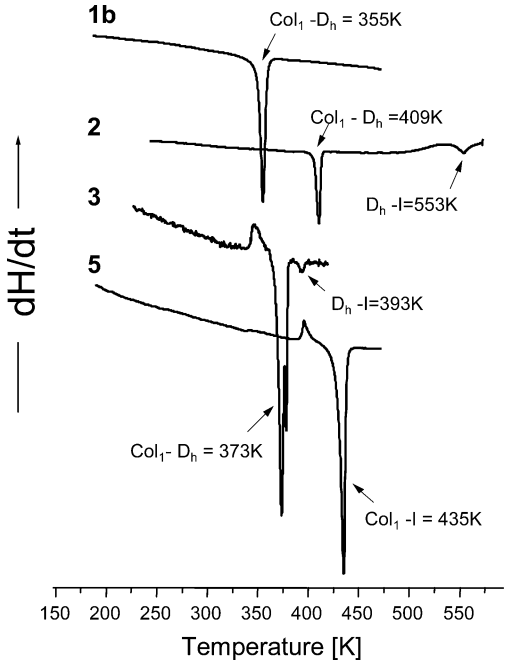

Figure 5. DSC traces (second heating run) of HBC−$C_{8,2}$ (**1b**), HBC−C_4−AQ (**2**), HBC−C_{11}−AQ (**3**), and HBC−(C_{11}−AQ)$_6$ (**5**). Heating rate 10 K/min. Transition temperatures from lower-temperature Col$_1$ phase to D$_h$ and isotropization temperatures are indicated.

act as a bound solvent that intercalates and destroys the HBC columns at the T_i.

Upon cooling to below their isotropization temperatures, compounds **1b**, **2**, **3**, **4**, and **6** all assemble to discotic hexagonal (D$_h$) mesophases, indicated by the WAXD equatorial intensity distributions (Supporting Information) containing the charac-

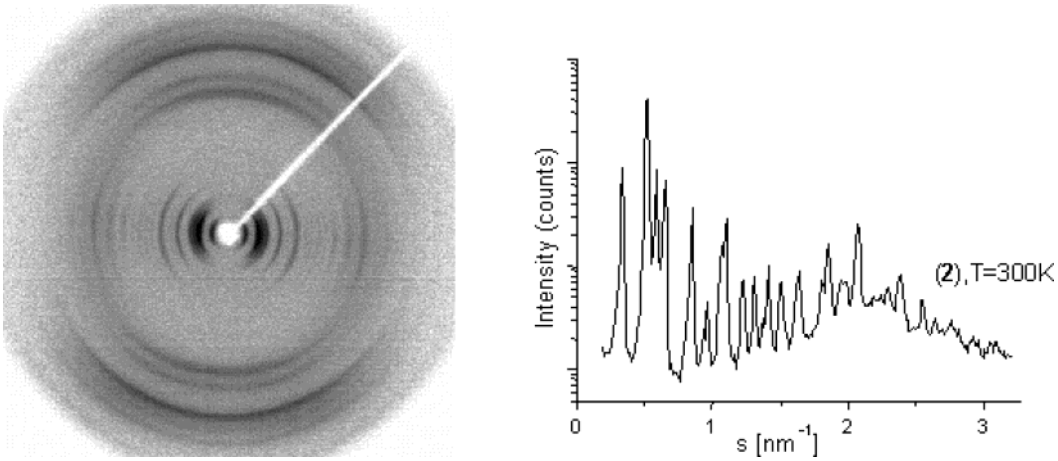

Figure 6. Two-dimensional WAXD diffractogram and equatorial integration obtained from oriented fiber of **2** in the room-temperature Col_1 phase. The intensities are plotted on a logarithmic scale.

Table 2. Thermal Data for **1**−**6**, Bulk Hexagonal Unit Cell Parameters *a*, and *d* spacings

		LC phase		
compound	$Col_1 \rightarrow D_h$ *T* (K)	*a* (nm)	d (nm) [*T* (K)]	T_i (K)
HBC−$C_{8,2}$, **1b**	355	2.644	0.368 [403]	693
HBC−C_4−AQ, **2**	409	2.76	0.38 [443]	553
HBC−C_{11}−AQ, **3**	373	2.618	0.367 [388]	393
HBC−C_4−DMA, **4**	342	2.67	[393]	598
HBC−$(AQ)_6$, **5**				435
HBC−C_4−Ac, **6**	357	2.56	0.366 [373]	710

teristic sequence of maxima with relative reciprocal spacings $\sqrt{1}$, $\sqrt{3}$, $\sqrt{4}$, and $\sqrt{7}$. The smallest angle reflection ([100] of the hexagonal lattice) is asymmetric and the baseline slopes for compounds **2**, **3**, and **4**, implicating greater lateral fluctuation of the disks spinning about the columnar axes,[23] associated with the tethered bulky units within the liquidlike alkyl sheaths. Single reflexes on the meridian at ∼0.36 nm (interplanar distance of graphite ∼0.34 nm) indicate that the disk planes are perpendicular to the columnar axes, without measurable intercalation by the tethered π-systems. Compound **5** shows no such highly mobile mesophase but instead passes directly from the isotropic phase to a solid "polycrystalline" phase on cooling. The six tethered AQs provide too much entropic disruption if mobile and/or act as excess bound solvent as proposed above. Slow cooling of thin isotropic films of **2**, **3**, and **4** between two glass slides causes homeotropic alignment, i.e., columns normal to the surfaces, as shown by optical microscopy (Supporting Information). This is common for columnar materials and would be highly desirable in photovoltaic devices since the columns would then provide the shortest and least tortuous possible percolation pathways across the junction between transparent electrode surfaces.

Upon sufficient cooling (below strong first-order endotherms in the DSC heating scans), the HBC disks of **2**, **3**, **4**, **5**, and **6** all tilt ("crystallize") within the columns by essentially the same angle (45−50°) as for model compound **1b**.[24] This tilt angle (Φ) is calculated from the symmetric meridianal reflections at $d \sim 0.5$ nm according to $\Phi = \arccos(\sim 0.35/\sim 0.5$ nm). In addition to changes in the equatorial intensity distributions conveying different intercolumnar packing, off-meridianal reflexes connote three-dimensional correlation between molecules resulting from decreased mobility. The room-temperature phases of all compounds are denoted as Col_1, rather than the standard K (crystalline) to avoid confusion. All dyads reported here could be plastically deformed at room temperature despite their "crystallized" π-systems, most likely due to amorphous side chains. The identical position of the meridianal reflexes for both AQ- and non-AQ-functionalized HBCs, and the lack of any others, indicate that the tethered π-systems are not intercalated in the HBC stacks. The question is then whether the tethered smaller π-systems are randomly distributed within the amorphous columnar jackets or are nanophase-separated. Increased thermal stability of the Col_1 phases of compounds **2**, **3**, and **5**, relative to models **1b** and **6**, indicate additional stabilizing interactions between AQ units. The slightly more bulky, and nonflat, DMA unit in **4** gives the opposite effect. Therefore, stabilization by the AQ units acting only as random, steric baffles hindering the onset of disk motion is unlikely. For compounds with undecanoyl spacers separating the HBC disks and the AQ units (**3** and **5**), cold recrystallization (first-order exotherm in DSC heating curve) immediately precedes the transition to the D_h phase for **3** and to the isotropic phase for **5**. This together with the greater thermal hysteresis of the $Col_1 \leftrightarrow D_h$ transitions of **2** and **3** compared to models **1a**,**b** and **6** also indicate that the AQs are not random spectators in the Col_1 phases. The tendency of pure AQ itself to crystallize could prevail here where AQ units from adjacent columns pair up to dimer "cross-links" or extended stacks.

A WAXD diffractogram characteristic of the room-temperature Col_1 phase of **2** is shown together with its integrated equatorial intensity distribution in Figure 6 (for remaining compounds, see Supporting Information). The relatively large number of equatorial reflexes allowed assignment of the lateral packing of the columns with high confidence to a 2D rhombic unit cell with parameters $a = 2.32$ nm, $b = 4.00$ nm, and $\alpha = 105.5°$. For space-filling reasons, this requires two molecules per unit cell. Which positions within this cell are occupied by HBC or AQ units cannot be inferred by WAXD of these mesomorphic (not single-crystalline) materials. The WAXD pattern of **3** gave much fewer and broader equatorial reflections that could still be assigned tentatively also as rhombic ($a =$

(23) Kettner, A.; Wendorff, J. H. *Liq. Cryst.* **1999**, *26*, 483−487.
(24) Bunk, O.; Nielsen, M. M.; Solling, T. I.; van de Craats, A. M.; Stutzmann, N. *J. Am. Chem. Soc.* **2003**, *125*, 2252−2258.

2.46 nm, $b = 4.01$ nm, and $\alpha = 102°$). The apparent shorter-range order of the Col_1 phase of **3** compared to that of **2**, consistent with lower thermal stability (DSC), indicates that the AQs do not play as significant a stabilizing role when separated by a longer alkyl tether. This is compatible with the STM results, where **3** yields more extended hexagonally packed domains, i.e., a smaller percentage of surface coverage by AQ units, which would otherwise give a unit cell of lower symmetry. Beyond that, the bulk 3D and the surface 2D packing cannot be compared, because the AQ units not lying flat on the surface in the 2D packing will not allow continuation of the 2D pattern into the third dimension, which is opposite to the previously published HBC−pyrene dyad, for which a good correlation between 2D and 3D arrangement was found. We have previously observed[25] a very similar bulk effect with carboxylic acid functions tethered to HBC disks by the same long and short alkyl chains. A short tether results in dramatic thermal stabilization of the room-temperature phase, whereas more randomized intercolumnar associations are likely with a longer tether.

Concluding Remarks

Novel acceptor−donor dyads based on HBC derivatives can self-assemble into nanophase-separated structures both in 2D at a surface and in 3D bulk columnar phases. The anthraquinone side groups play a diminished role in the packing at surfaces, compared to a previously published HBC−pyrene dyad[10] and also compared to their own behavior in the bulk. Within the monolayers, the AQs might inter- or intramolecularly stack on top of HBC cores or be partially solvated in the 3D supernatant solution as well as assemble on the HOPG substrate, defining the size of apparent voids. This behavior contrasts to the highly ordered monolayers formed from the hexa-AQ-substituted HBC **5**, most likely due to space-filling considerations compensating for increased dynamics. Success in patterning surfaces with covalent donor−acceptor couples depends on chemical structure of the individual components, their incorporation ratio in the molecules, and undoubtedly on the processing conditions (e.g., utilization of a solvent less competitive for the surface). The self-assembled, well-defined arrangement of substantially different molecular electronic units reported here paves the way toward their simultaneous electrical characterization by scanning tunneling spectroscopy, which is currently underway. Moving from 2D to 3D, comparison of the thermotropic behavior of the new HBC−AQ compounds to that of model compounds without AQ units indicates phase separation of the acceptor units in a regular fashion from the donor HBC columns. Homeotropic alignment was demonstrated whereby the columns could eventually be used to provide one-dimensional charge transport between flat transparent electrodes as desired in pholtovoltaic diodes. We continue in a stepwise approach by preparing HBC−acceptor dyads with larger acceptor components for a greater tendency toward face-to-face stacking, which should more highly favor independent acceptor column formation, and/or those that possess optoelectronic properties more suitable for exploitation of the solar spectrum, e.g., rylene chromophores and C_{60}-fullerenes.

Acknowledgment. This work was supported by EU Projects SISITOMAS, MAC-MES, and DISCEL (Contract G5RD-CT2000-00321), the Volkswagen-Stiftung (Elektronentransport durch konjugierte molekulare Scheiben und Ketten), the European Science Foundation through the programs SMARTON and SONS-BIONICS, and the German "Bundesministerium für Forschung und Technologie" as part of the program "Zentrum für multifunktionelle Werkstoffe und miniaturisierte Funktionseinheiten" (BMBF 03N 6500).

Supporting Information Available: Full synthetic and experimental details, solution photoluminescence and excitation spectra, additional WAXD data, and temperature-dependent optical micrographs (PDF). This material is available free of charge via the Internet at http://pubs.acs.org.

JA038648+

(25) Tchebotareva, N. Functionalized Hexa-peri-hexabenzocoronene: Synthesis and Supramolecular behavior. Ph.D. Dissertation, Johannes Gutenberg University, Mainz, Germany 2003.